JASA ARTICLE

Acoustic imaging using unknown random sources

Aaron C. Prunty,[1,a)] Roel K. Snieder,[1,b)] and Christoph Sens-Schönfelder[2]
[1]*Department of Geophysics, Colorado School of Mines, Golden, Colorado 80401, USA*
[2]*Helmholtz Centre Potsdam–GFZ German Research Centre for Geosciences, Potsdam, Germany*

ABSTRACT:
We investigate the feasibility of imaging localized velocity contrasts within a nonattenuating acoustic medium using volume-distributed random point sources. We propose a simple, two-step processing flow that utilizes the linear sampling method to invert for the target locations directly from the recorded waveforms. We present several proof-of-concept experiments using Monte Carlo simulations to generate independent realizations of band limited "white noise" sources, which are randomly distributed in both time and space. Despite the unknown and random character of the illumination on the imaging targets, we show that it is possible to image strong velocity contrasts directly from multiply scattered coda waves in the recorded data. We benchmark the images obtained from the random-source experiments with those obtained by a standard application of the linear sampling method to analogous controlled-source experiments.
© *2021 Acoustical Society of America*. https://doi.org/10.1121/10.0003334
(Received 20 October 2020; revised 11 November 2020; accepted 17 December 2020; published online 22 January 2021)
[Editor: Karim G. Sabra] Pages: 499–507

I. INTRODUCTION

Imaging is a process that seeks to reconstruct the unknown spatial distribution of one or more properties of a medium. For example, in underwater acoustics, one may seek to determine the distribution of sound speed in a water column or density variations within a seabed (Rajan and Frisk, 2020). The idea is to illuminate the medium using one or more sources of acoustic waves, and then measure the medium's response to this illumination at an array of receivers. An image of the medium is subsequently obtained by performing a choice set of operations on the recorded responses—usually in conjunction with an assumed model of the medium—to deduce the spatial distribution of the medium's properties. For example, the model may represent a "smooth" estimate of the real medium, and the operations used to obtain an image are chosen to extract higher-resolution details from the recorded data (Etgen *et al.*, 2009).

In some applications, one may desire to image a small subset of the medium only. An example is time-lapse seismic monitoring, where one seeks to track temporal variations in rock properties or fluid distributions within a hydrocarbon reservoir (e.g., Grêt *et al.*, 2006; Lumley, 2001; Vasco, 2004; Vasco *et al.*, 2004); it is unnecessary—and inefficient—to image the medium outside the area of interest. Imaging methods capable of localizing features (or "targets") within a specified subset of the medium are commonly referred to as "target-oriented." Ayeni and Biondi (2010) and Asnaashari *et al.* (2015) give strategies for target-oriented imaging and inversion of time-lapse seismic data.

Traditional imaging requires that the sources of the wave field are known and available to operate under economical constraints. We consider the opposite case where the sources of energy are unknown, uncontrolled, and of a random character, and propose a target-oriented imaging workflow to image an acoustic medium under such challenging conditions. The workflow consists of an amplitude normalization of the recorded data followed by an inversion for the target locations using the linear sampling method. As a proof-of-concept study, we present the workflow in the context of imaging velocity perturbations in a nonattenuating acoustic medium. For clarity in what follows, we refer to "primary sources" as those that create acoustic energy and to "secondary sources" as those that redistribute acoustic energy (e.g., scatterers). Additionally, we refer to a source as "known" if both its space and time dependence are known or directly observable; otherwise, we refer to a source as "unknown."

Conventional imaging methods assume that the sources used to interrogate a medium are known, controlled, and—to as much an extent as possible—emit a predictable and repeatable source signature [e.g., Kirchhoff migration (Bleistein, 1987; Schneider, 1978) and reverse-time migration (Baysal *et al.*, 1983; McMechan, 1983)]. In these methods, it is assumed that the space and time dependence of the sources are known so that the wave fields produced by them can be effectively modeled. In a separate but related problem, velocity estimation techniques such as full-waveform inversion (Tarantola, 1984; Virieux and Operto, 2009) also assume the sources are known.

Ambient-noise seismology relies on waves that are generated by unknown and uncontrolled sources, such as ocean

[a)]Author to whom all correspondence should be addressed: prunty@mines.edu, ORCID: 0000-0003-2822-5220.
[b)]ORCID: 0000-0003-1445-0857.

waves, city traffic, factories, and microearthquakes that surround the domain to be investigated (e.g., Artman, 2006; Curtis *et al.*, 2006; Girard and Shragge 2019a, 2019b; Larose *et al.*, 2006; Sabra *et al.*, 2005; Shapiro and Campillo, 2004; Shapiro *et al.*, 2005; Snieder and Larose, 2013). Despite not knowing the details of the sources, seismic interferometry can be applied to extract the impulse response that propagates between a pair of receivers, provided the ambient sources are uncorrelated and uniformly distributed around the receivers (Draganov *et al.*, 2004; Halliday and Curtis, 2008; Sens-Schönfelder and Wegler, 2006). The obtained impulse response can then be used to construct an image of the medium (for example, by using one of the migration methods referenced above). Fichtner *et al.* (2017) provide a generalized approach to seismic interferometry in which they invert for a function that characterizes the primary sources of the wave field, and the intermediate step of extracting the medium's impulse response is avoided. However, their approach cannot be used to localize secondary sources (such as scatterers), since scatterers are on average temporally correlated and their assumption [Eq. (9)] will not hold.

While seismic interferometry eliminates the need to know the details of the sources for many practical cases, it does have limitations that make it unsuitable for cases when the sources of the wave field are dispersed throughout the medium. In particular, seismic interferometry extracts the waves that propagate between different receivers by cross-correlating the waveforms recorded at different receivers (Curtis *et al.*, 2006; Larose *et al.*, 2006; Lobkis and Weaver, 2001; Roux *et al.*, 2004; Sabra *et al.*, 2008; Snieder and Larose, 2013). For acoustic waves in nonattenuating media, the theory requires that the sources are located on a surface enclosing the receivers and that there are no back-scattered waves propagating inward through this surface (Wapenaar *et al.*, 2005). The application of seismic interferometry to attenuating acoustic media requires noise sources on a bounding surface, as well as in the interior of this surface in a proportion dictated by the attenuation (Snieder, 2007). It is for diffusive systems that one only needs sources in the interior of the medium (Snieder, 2006). In general, the application of seismic interferometry to physical systems that are invariant under time reversal requires that noise sources are located on a surface surrounding the receivers and that when the invariance for time reversal is broken one also needs sources throughout the volume (Snieder *et al.*, 2007). The imaging method we present here employs nonattenuating acoustic waves that are generated by unknown sources distributed throughout the medium. In fact, the sources are interspersed amongst the scatterers we seek to image. On the one hand, this source distribution violates the key assumptions of seismic interferometry for nonattenuating media, and so an alternative imaging method must be found. On the other hand, this source distribution may provide better illumination on the scatterers than sources that surround the medium.

As an alternative to seismic interferometry, we investigate the linear sampling method (Chen *et al.*, 2010; Colton and Kirsch, 1996; Colton *et al.*, 1997; Guo *et al.*, 2013; Haddar *et al.*, 2014; Prunty and Snieder, 2019), which is a target-oriented imaging procedure for localizing scatterers within a known background medium. The linear sampling method is related to the Lippmann-Schwinger inversion, wherein one inverts for the source of the scattered waves using the properties of the background medium (Prunty and Snieder, 2020). In the linear sampling method, one attempts to extract from the measured scattered waves a single impulse response that radiates from a given point in the background medium (Chen *et al.*, 2010; Colton and Kirsch, 1996; Colton *et al.*, 1997; Guo *et al.*, 2013; Haddar *et al.*, 2014; Prunty and Snieder, 2019). A key characteristic of the method is that it is agnostic to the physical properties and boundary conditions imposed by the unknown scatterers (e.g., see Tacchino *et al.*, 2002, and the references therein). Consequently, no weak-scattering approximation is necessary.

As a data-driven imaging procedure, the linear sampling method extracts the space and time dependence of a scatterer from the recorded waveforms. Consequently, the space and time dependence of the illumination on the imaging targets need not be known. In fact, no information pertaining to the sources (whether known or not) is used in the inversion by the linear sampling method. This makes the linear sampling method an appealing candidate for imaging in the presence of unknown and uncontrolled random sources. To our knowledge, the linear sampling method has never been tested on data acquired under such conditions.

In what follows, we demonstrate the feasibility of imaging localized scatterers within a nonattenuating acoustic medium using unknown random sources. We present the essential information needed to formulate the linear sampling method for the case of random sources in Sec. II and demonstrate the workflow with numerical experiments in Sec. III. We conclude with a discussion of the numerical experiments and remaining challenges in Sec. IV.

II. METHODOLOGY

Our goal is to image unknown, arbitrary scatterers embedded within a known background medium using unknown and uncontrolled random sources. In the examples shown here, the background medium is homogeneous, but it can be inhomogeneous. Our strategy is to apply the linear sampling method to image the scatterers directly from the total recorded waveforms, without first extracting the perturbed medium's impulse response. Our only assumption about the sources is that they are transient on the timescale of the recording period of the experiment. In what follows, we use boldface letters to denote measured (discrete) quantities.

Suppose we make a number of recordings of the total pressure field in an acoustic medium in which ambient, unknown sources go off randomly in time and space. The observed pressure field then consists of direct waves that propagate between the random sources and the receivers, as

https://doi.org/10.1121/10.0003334

well as scattered waves that are radiated by inhomogeneities within the medium. These scatterers act as secondary sources, whose time dependence varies with that of the random illumination. Whereas the random sources go off unpredictably throughout the medium, the scatterers radiate energy consistently from their fixed locations. As we show momentarily, this fact is key for the linear sampling method to image the scatterers.

Let $\mathbf{p}_j$ denote the pressure field measured in record j at receiver positions $\mathbf{x}_i$, where $i = 1, \ldots, N_r$ and N_r is the number of receivers. In the linear sampling method, we create a search domain (or imaging domain) in which we seek to reconstruct the shape of the unknown scatterers (Colton and Kirsch, 1996; Colton *et al.*, 1997). To do this, the linear sampling method posits a relation between the recorded data $\mathbf{p}_j$ and an impulse response of the background medium from each point $\mathbf{z}$ in the search domain. Formally, this relation is realized as an ill-posed linear system of equations. Let $\mathbf{G_z}$ denote the impulse response of the background medium observed at the receivers $\mathbf{x}_i$ from a given point $\mathbf{z}$ in the search domain. For each point $\mathbf{z}$, we seek an approximate solution to this ill-posed system of equations by minimizing the least squares objective function

$$\min_{\boldsymbol{\varphi}_\mathbf{z}} \{||\mathbf{N}\boldsymbol{\varphi}_\mathbf{z} - \mathbf{G_z}||^2 + \alpha||\boldsymbol{\varphi}_\mathbf{z}||^2\} \tag{1}$$

for $\boldsymbol{\varphi}_\mathbf{z}$. In this expression, the last term regularizes the minimization and $\alpha \geq 0$ is a regularization parameter. The operator $\mathbf{N}$ denotes a time convolution with the recorded data $\mathbf{p}$. In the frequency domain, its action on an arbitrary vector $\mathbf{g}$ is defined by

$$\mathbf{Ng} = \sum_j \mathbf{p}_j(\mathbf{x}_i, \omega)\mathbf{g}(j, \omega), \tag{2}$$

where ω denotes the angular frequency. The least squares solution to Eq. (1) exhibits a peculiar "blowup behavior" that indicates the presence (or absence) of a scatterer (Colton and Kirsch, 1996; Colton *et al.*, 1997): the norm of the solution $||\boldsymbol{\varphi}_\mathbf{z}||$ becomes arbitrarily large whenever $\mathbf{z}$ is outside the scatterers, and is bounded otherwise. It can be shown that the blowup behavior results from a division by zero in the unregularized linear system [Eq. (1)], since the solution $\boldsymbol{\varphi}_\mathbf{z}$ is inversely proportional to the source of the scattered field, which is identically zero outside the scatterers (Prunty and Snieder, 2019).

We define the image at each point in the search domain by

$$I(\mathbf{z}) = \frac{f(\mathbf{z}) - \min f(\mathbf{z})}{\max f(\mathbf{z}) - \min f(\mathbf{z})}, \tag{3}$$

where

$$f(\mathbf{z}) = \frac{1}{||\boldsymbol{\varphi}_\mathbf{z}||}. \tag{4}$$

That is, the image at a point $\mathbf{z}$ is defined to be a number between 0 and 1, where a value close to 1 indicates the point is likely inside the scatterer and a value close to 0 indicates otherwise.

Note that the impulse response appearing in Eq. (1) should reflect the monopole and/or dipole nature of the imaging target. For example, velocity contrasts act as monopole sources, whereas density contrasts act as dipole sources. In general, acoustic media feature both types of scatterers, so a combination of monopole and dipole impulse responses will be needed for imaging. In Sec. III, we focus on a special case of imaging velocity contrasts in an otherwise homogeneous acoustic medium. Consequently, $\mathbf{G_z}$ in Eq. (1) will be the impulse response due to a monopole point source in the background medium.

The application of the operator $\mathbf{N}$ in Eq. (2) involves a summation over data records j. This implies that the linear sampling method will image a source (primary or secondary) at the point $\mathbf{z}$ if, on average over many observations, it radiates a wave from the point $\mathbf{z}$. Because the random sources go off unpredictably in space and are unlikely to repeat from one data record to the next, they are unlikely to be imaged by the linear sampling method. In contrast, the scatterers radiate waves consistently from their fixed locations and, in principle, should be well imaged by the linear sampling method. A problem arises, however, when the scattered radiation is weak compared to other waveforms present in the data. In particular, the contribution of the random sources to the measured signal may still dominate that of the scatterers.

In a least squares sense, the linear sampling method inverts for the sources of the signals with the largest amplitudes (i.e., signals produced by sources with the most energy). This means that in a random-source experiment, in which direct arrivals between the random sources and receivers dominate the recorded waveforms, the linear sampling method first and foremost attempts to image the random sources and not the scatterers of interest. In order for the method to "see" the scattered waves, it is necessary to boost their amplitudes relative to those of the direct waves. Using the fact that the direct waves are of large amplitude but relatively short duration (in contrast to the scattered waves, which are weak but persistent in time), we apply a running-absolute-mean normalization to each receiver trace (Bensen *et al.*, 2007). If we denote by $p_j(\mathbf{x}_i, t_n)$ the pressure field measured in record j at location $\mathbf{x}_i$ and at time t_n, then the normalization is computed as

$$\tilde{p}_j(\mathbf{x}_i, t_n) = \frac{p_j(\mathbf{x}_i, t_n)}{w_n + \epsilon}, \tag{5}$$

where

$$w_n = \frac{1}{2N+1} \sum_{k=n-N}^{n+N} |p_j(\mathbf{x}_i, t_k)| \tag{6}$$

is the running absolute mean over the time window of length $2N + 1$ centered at time t_n, and ϵ is a "small" positive constant introduced to regularize the normalization during

quiescent periods in the time series (in which w_n may approach zero). Bensen *et al.* (2007) discuss the influence of the window length on the normalization; we choose the integer N such that the window length $2N+1$ equals the number of time samples contained in the maximum period (or lowest frequency) of the observed signal. Once a satisfactory normalization is obtained, we replace $\mathbf{p}$ in Eq. (2) with the normalized data $\tilde{\mathbf{p}}$. As a rule of thumb, the thresholding parameter ϵ should be much smaller than a typical running absolute mean w_n in sections of a trace where signal clearly exists, but still large enough so that unwanted noise is not over-boosted in sections of the trace where there is no identifiable signal. In our numerical experiments described in Sec. III, we found the root mean square (RMS) amplitude of the data across all imaging experiments to be $O(10^{-7})$. Using a trial-and-error approach to estimate the thresholding parameter, we found that $\epsilon = O(10^{-9})$ yielded a satisfactory normalized trace in which the amplitudes of multiply scattered waves and direct arrivals from the random sources were balanced, while also ensuring that numerical errors to due finite accuracy of our modeling code were not over-boosted. We illustrate our normalization with several examples in Sec. III.

III. NUMERICAL EXPERIMENTS

A. Modeling scatterers in a two-dimensional, homogeneous acoustic medium

To test our methodology, we model the scattering of pressure fields in a two-dimensional, unbounded, nonattenuating acoustic medium of constant density and variable velocity. We assume the pressure fields are generated by monopole (isotropically radiating) point sources. For a given source that goes off at location $\mathbf{x}_s$ and at time t_s, we obtain the resulting pressure field p by solving our model wave equation

$$\nabla^2 p(\mathbf{x},t) - \frac{1}{c^2(\mathbf{x})}\frac{\partial^2 p(\mathbf{x},t)}{\partial t^2} = -\delta(\mathbf{x}-\mathbf{x}_s)S(t-t_s), \quad \mathbf{x}\in\mathbb{R}^2, \quad 0\le t\le T, \tag{7}$$

together with the initial conditions

$$p(\mathbf{x},t) = 0, \quad \frac{\partial p(\mathbf{x},t)}{\partial t} = 0, \quad \mathbf{x}\in\mathbb{R}^2, \quad t < t_s. \tag{8}$$

In Eq. (7), c is the spatially varying velocity we seek to image, δ is the Dirac delta function that localizes the point source, and S is a given source-time function that generates the pressure disturbance. The times $t=0$ and $t=T$ are the start and end time of a recording period, respectively. We solve Eq. (7) using a finite-difference scheme implemented in the Madagascar open-source software package (Fomel *et al.*, 2013), which is freely available at http://www.ahay.org. Because Eq. (7) is linear in the unknown variable p, the pressure field resulting from a more general distribution of sources (e.g., a random distribution of point sources) is obtained by summing the pressure fields due to each individual source.

Figure 1(a) shows the modeling domain in which we solve Eq. (7), as well as the general setup of our imaging experiments. We use absorbing boundary conditions to prevent reflections off the edges of the model. The shape of the imaging target is given by the letters "CWP," and is embedded within a background medium of constant wave speed $c_0 = 2$ km/s; we describe "strong" and "weak" scattering scenarios for the velocity function inside the imaging target in Sec. III B. Randomly distributed sources, shown as the white dots in Fig. 1(a), illuminate the imaging target from all directions. The total pressure field is measured at 50 receivers placed along a circle of radius 8 cm, which fully encloses the imaging target. The recording period for the experiments is 400 μs.

B. Monte Carlo parameterization of the random-source imaging experiments

To simulate unknown and uncontrolled random sources, we use the following Monte Carlo approach: the number of sources present in a given recording period is a random integer uniformly distributed between 2 and 10; the locations of the sources are uniformly distributed within the domain of

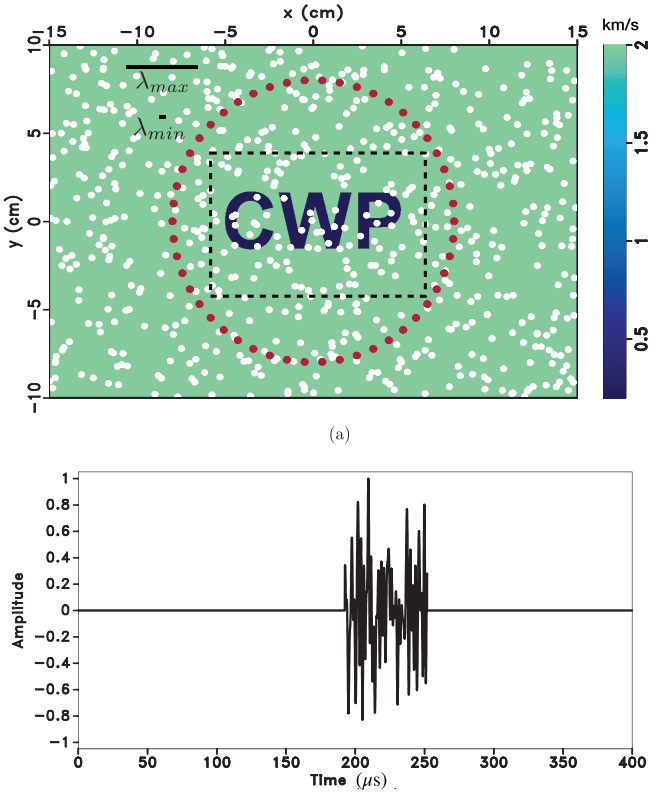

FIG. 1. (Color online) (a) Experimental setup of the imaging problem. Random sources are shown as white dots, receivers as red dots, and the imaging domain by the black dashed line. In this example, about 630 sources were generated during the experiment. The model shown is for the strong velocity contrast. (b) A typical noise source simulated in the experiment. The minimum and maximum wavelengths contained in the noise are shown as λ_{min} and λ_{max}, respectively, in panel (a).

https://doi.org/10.1121/10.0003334

the model; each source emits a distinct "white noise" in the frequency band of 50 to 600 kHz; the duration of a noise source is uniformly distributed between 10% and 20% of the recording period; the time at which a source goes off is uniformly distributed between 5% and 60% of the recording period. Thus, the sources emit different noise realizations, of different durations, at different times, and from different points in the medium. An example noise source is shown in Fig. 1(b). The corresponding minimum and maximum wavelengths contained in the noise are shown for scale in Fig. 1(a). The receivers are in the near field of the imaging target for lower-frequency components of the noise, and in the far field of target for higher-frequency components.

Given the above Monte Carlo parameterization, we conduct our random-source imaging experiments as follows:

1. Specify the number of recordings M for the given experiment.
2. Run M independent Monte Carlo simulations to generate and record the wave fields from random sources.
3. Apply the running-absolute-mean normalization to each data record.
4. Apply the linear sampling method to the normalized dataset.

In what follows, we perform four independent random-source experiments, wherein the number of recordings are $M = 25$, 50, 75, and 100. For the experiment with 100 recordings, our Monte Carlo parameterization allows the total number of sources generated during the experiment to be anywhere between 200 and 1000. To test the ability of the linear sampling method to image both weak scatterers and strong scatterers in the presence of random sources, we model two cases for the velocity of the scattering target. In the weak scattering case, the velocity of the scatterer is set to 2.2 km/s (a 10% increase from the background velocity). In the strong scattering case, the velocity of the scatterer is set to 0.2 km/s (a 90% decrease from the background velocity).

C. Setup for the linear sampling method

We image the medium in the search domain $[-6\,\text{cm}, 6\,\text{cm}] \times [-4\,\text{cm}, 4\,\text{cm}]$ within the xy-plane, shown as the black dashed line in Fig. 1(a). We discretize the search domain into a 60×40 point regularly sampled grid and model the impulse response of the background medium $\mathbf{G_z}$ from each grid point $\mathbf{z}$ using a 300 kHz Ricker pulse. For our two-dimensional background model, this amounts to evaluating the analytic function

$$\boldsymbol{G}_{\mathbf{z}}(\mathbf{x}_i, \tau) = \frac{\zeta(\tau) H(\tau - ||\mathbf{x}_i - \mathbf{z}||/c_0)}{2\pi\sqrt{\tau^2 - ||\mathbf{x}_i - \mathbf{z}||^2/c_0^2}}, \quad -T \le \tau \le T, \tag{9}$$

at the receiver locations $\mathbf{x}_i$ [recall from Eqs. (1) and (2) that $\boldsymbol{G}_{\mathbf{z}}$ is set to be a time convolution of the recorded data—hence, τ lies between $-T$ and T]. In Eq. (9), H is the Heaviside (unit step) function, and ζ is the Ricker pulse

$$\zeta(\tau) = \left[1 - 2\pi^2\nu^2(\tau - 0.1)^2\right] e^{-\pi^2\nu^2(\tau-0.1)^2} \tag{10}$$

with peak frequency $\nu = 300$ kHz.

D. Benchmarking against controlled-source analogues

To check the performance of our proposed workflow, we compare the images obtained from the random-source experiments with those that would have been obtained from a standard application of the linear sampling method to an analogous controlled-source experiment. In this case, the linear sampling method inverts for the scatterer locations using the difference between the pressure fields measured in the perturbed and unperturbed media, respectively (here, the perturbed medium contains the scatterer and the unperturbed medium is the assumed background model). To perform this controlled-source experiment, we co-locate a "known" source with each receiver shown in Fig. 1(a), again using the 300 kHz Ricker pulse [Eq. (10)] as a source-time function. For each source, we simulate the pressure fields in both

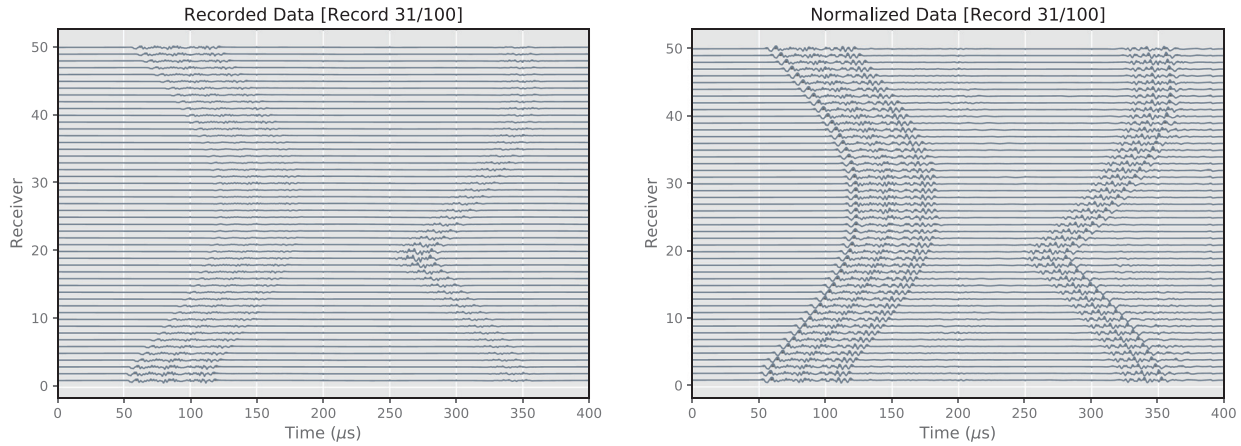

(a) (b)

FIG. 2. (Color online) (a) A typical data record from a random-source experiment in the weakly scattering medium. (b) The same data record after normalization.

the perturbed and unperturbed media, record the waveforms observed at the 50 receiver locations, and then take the difference between the two sets of measurements. We invert for the target locations by applying the linear sampling method to the remaining scattered fields only.

E. Case I: Weak velocity contrast

Figure 2(a) shows a data record from a random-source experiment in the weakly scattering medium. In this example, two direct arrivals are observed well separated in time. Figure 2(b) shows the same data record after running-absolute-mean normalization. A comparison between Figs. 2(a) and 2(b) suggests that little scattered energy is present in the original data, as few scattered arrivals become apparent after normalization at times between the direct arrivals.

Figure 3 shows the images obtained by the linear sampling method for the different random-source experiments in the weakly scattering medium, as well as the benchmark image from the analogous controlled-source experiment. In all

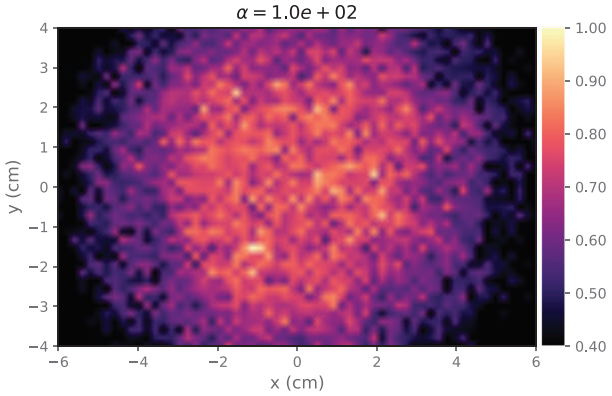

(a) 25 records

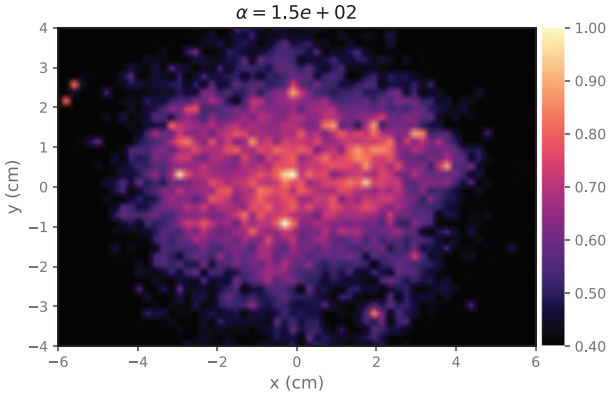

(b) 50 records

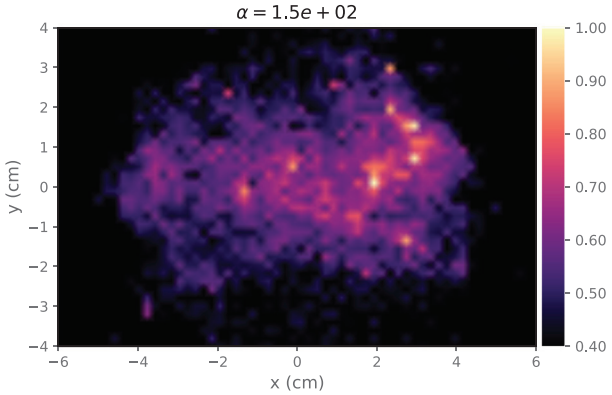

(c) 75 records

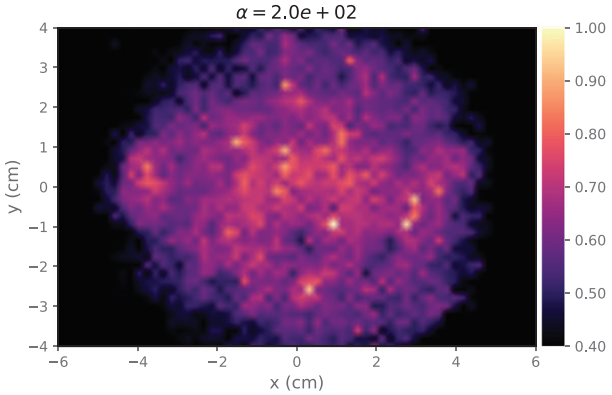

(d) 100 records

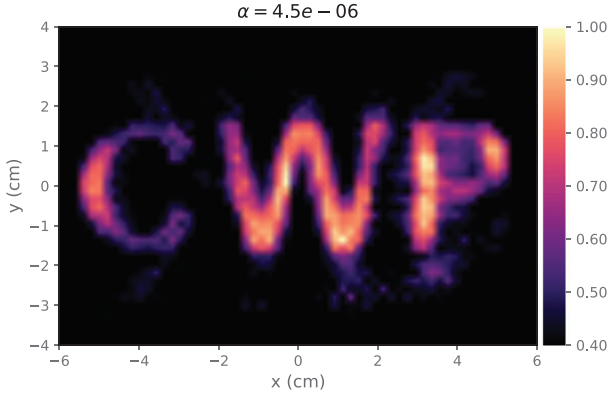

(e) Controlled-source benchmark

FIG. 3. (Color online) (a–d) Reconstructions of the CWP letters obtained for the random-source experiments in the weakly scattering medium. (e) Benchmark image obtained for the controlled-source experiment. The value of the regularization parameter α is indicated above each plot.

https://doi.org/10.1121/10.0003334

of the random-source experiments, the method failed to image the CWP letters, but identified a few of the random sources present within the imaging domain [shown as the bright spots in Figs. 3(a)–3(d)]. This is not surprising: since the velocity contrast is weak, there is little to no scattered energy in the recorded data that could be amplified from the normalization. Hence, the scatterer is not detected. In Fig. 3(e), the benchmark image obtained from the controlled-source experiment more clearly reconstructs the CWP letters.

F. Case II: Strong velocity contrast

Figure 4 shows a data record from a random-source experiment in the strongly scattering medium before and after normalization. Here, the amplification of multiply scattered waves at times between the direct arrivals is apparent.

Figure 5 shows the images obtained by the linear sampling method for the different random-source experiments in the strongly scattering medium, as well as the benchmark image from the analogous controlled-source experiment. Unlike for the case of the random-source experiments in the weakly scattering medium, here the linear sampling method was able to reconstruct a rough estimate of the CWP letters from the normalized data. In this case, however, the random primary sources are not imaged. We attribute this to the fact that strongly scattering media create scattered waves of longer duration which, after normalization, impose a stronger constraint on the scatterer location.

Interestingly, the benchmark image shown in Fig. 5(e) obtained from the controlled-source experiment shows the CWP letters less clearly than those obtained from the random-source experiments shown in Figs. 5(a)–5(d). In particular, the linear sampling method appears to detect only the outermost boundaries of the letters in the controlled-source experiment. Physically, this is likely due to weak transmission caused by the strong velocity contrast: most of the energy approaching from the exterior of the letters does not transmit through the letters. Finally, there is the fact that the random-source experiments contain many more sources of energy than the controlled-source experiments and, in particular, sources that provide illumination between the letters. Consequently, the interior of the CWP letters is better illuminated in the random-source experiments than in the controlled-source experiments, a fact which certainly impacts the quality of the image.

IV. DISCUSSION AND CONCLUSIONS

We have shown that it is possible to image strong velocity contrasts within a nonattenuating acoustic medium in the presence of random point sources whose locations and source-time functions are unknown. The obtained images are of relatively low resolution, which is not surprising given the challenging conditions of this inverse problem. The success of our approach lies in the fact that strongly scattering targets generate a persistent coda of scattered energy that can be detected and amplified during intermittent periods between the relatively large (but transient) arrivals from random noise sources. As demonstrated in Sec. III, weakly scattering targets do not generate such coda waves and are therefore more difficult to image under the conditions of our experiment.

Opportunities for further research include generalizing the proposed workflow to accommodate other types of media and imaging targets, such as weakly attenuating acoustic and elastic media. To this end, we note that the linear sampling method is already well established for elastic media (e.g., Anagnostopoulos and Charalambopoulos, 2006; Arens, 2001; Charalambopoulos *et al.*, 2002; Fata and Guzina, 2004; Guzina and Madyarov, 2007). As a direct consequence of our assumption that the noise sources are transient, we cannot apply our proposed workflow to image targets using continuous sources, such as the "hum" of a factory or wind turbine (Gassenmeier *et al.*, 2014). Finally, data acquired in a laboratory or field experiment often have various noises that must be suppressed before imaging. We suspect careful consideration will need to be taken when

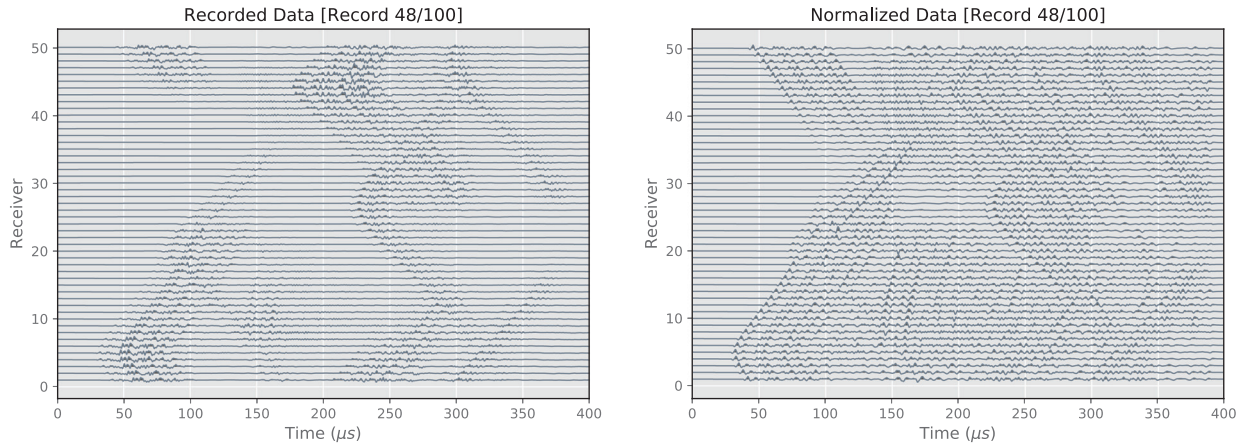

FIG. 4. (Color online) (a) A typical data record from a random-source experiment in the strongly scattering medium. (b) The same data record after normalization.

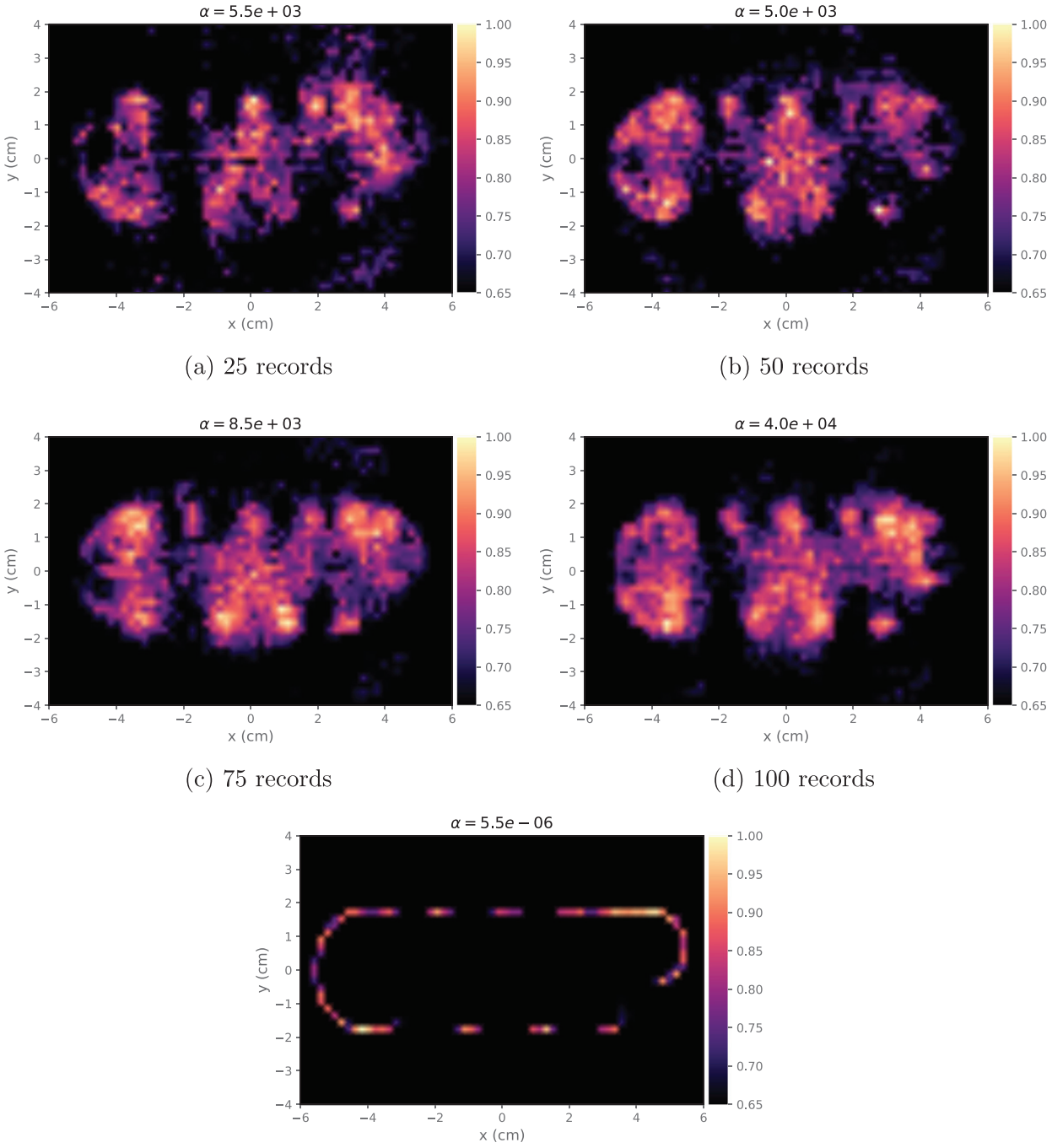

(a) 25 records (b) 50 records

(c) 75 records (d) 100 records

(e) Controlled-source benchmark

FIG. 5. (Color online) (a–d) Reconstructions of the CWP letters obtained for the random-source experiments in the strongly scattering medium. (e) Benchmark image obtained for the controlled-source experiment. The value of the regularization parameter α is indicated above each plot.

denoising the data and choosing the thresholding parameter for normalization.

ACKNOWLEDGMENTS

We thank Kees Wapenaar and an anonymous reviewer for their constructive feedback. This work was supported by the Consortium Project on Seismic Inverse Methods for Complex Structures at the Colorado School of Mines.

Anagnostopoulos, K. A., and Charalambopoulos, A. (**2006**). "The linear sampling method for the transmission problem in 2D anisotropic elasticity," Inverse Problems **22**(2), 553–577.

Arens, T. (**2001**). "Linear sampling methods for 2D inverse elastic wave scattering," Inverse Problems **17**(5), 1445.

Artman, B. (**2006**). "Imaging passive seismic data," Geophysics **71**(4), SI177–SI187.

Asnaashari, A., Brossier, R., Garambois, S., Audebert, F., Thore, P., and Virieux, J. (**2015**). "Time-lapse seismic imaging using regularized full-waveform inversion with a prior model: Which strategy?," Geophys. Prospect. **63**(1), 78–98.

Ayeni, G., and Biondi, B. (**2010**). "Target-oriented joint least-squares migration/inversion of time-lapse seismic data sets," Geophysics **75**(3), R61–R73.
Baysal, E., Kosloff, D. D., and Sherwood, J. W. (**1983**). "Reverse time migration," Geophysics **48**(11), 1514–1524.
Bensen, G., Ritzwoller, M., Barmin, M., Levshin, A., Lin, F., Moschetti, M., Shapiro, N., and Yang, Y. (**2007**). "Processing seismic ambient noise data to obtain reliable broad-band surface wave dispersion measurements," Geophys. J. Int. **169**(3), 1239–1260.
Bleistein, N. (**1987**). "On the imaging of reflectors in the earth," Geophysics **52**(7), 931–942.
Charalambopoulos, A., Gintides, D., and Kiriaki, K. (**2002**). "The linear sampling method for the transmission problem in three-dimensional linear elasticity," Inverse Problems **18**(3), 547.
Chen, Q., Haddar, H., Lechleiter, A., and Monk, P. (**2010**). "A sampling method for inverse scattering in the time domain," Inverse Problems **26**(8), 085001.
Colton, D., and Kirsch, A. (**1996**). "A simple method for solving inverse scattering problems in the resonance region," Inverse Problems **12**(4), 383–393.
Colton, D., Piana, M., and Potthast, R. (**1997**). "A simple method using Morozov's discrepancy principle for solving inverse scattering problems," Inverse Problems **13**(6), 1477–1493.
Curtis, A., Gerstoft, P., Sato, H., Snieder, R., and Wapenaar, K. (**2006**). "Seismic interferometry: Turning noise into signal," Leading Edge **25**, 1082–1092.
Draganov, D., Wapenaar, K., and Thorbecke, J. (**2004**). "Passive seismic imaging in the presence of white noise sources," Leading Edge **23**(9), 889–892.
Etgen, J., Gray, S. H., and Zhang, Y. (**2009**). "An overview of depth imaging in exploration geophysics," Geophysics **74**(6), WCA5–WCA17.
Fata, S. N., and Guzina, B. B. (**2004**). "A linear sampling method for near-field inverse problems in elastodynamics," Inverse Problems **20**(3), 713.
Fichtner, A., Stehly, L., Ermert, L., and Boehm, C. (**2017**). "Generalized interferometry - I: Theory for interstation correlations," Geophys. J. Int. **208**(2), 603–638.
Fomel, S., Sava, P., Vlad, I., Liu, Y., and Bashkardin, V. (**2013**). "Madagascar: Open-source software project for multidimensional data analysis and reproducible computational experiments," J. Open Res. Software **1**(1), e8.
Gassenmeier, M., Sens-Schönfelder, C., Delatre, M., and Korn, M. (**2014**). "Monitoring of environmental influences on seismic velocity at the geologic storage site for CO_2 in Ketzin (Germany) with ambient seismic noise," Geophys. J. Int. **200**, 524–533.
Girard, A. J., and Shragge, J. (**2019a**). "Automated processing strategies for ambient seismic data," Geophys. Prospect. **68**, 293–312.
Girard, A. J., and Shragge, J. (**2019b**). "Direct migration of ambient seismic data," Geophys. Prospect. **68**, 270–292.
Grêt, A., Snieder, R., and Scales, J. (**2006**). "Time-lapse monitoring of rock properties with coda wave interferometry," J. Geophysical Res.: Solid Earth **111**(B3), B03305.
Guo, Y., Monk, P., and Colton, D. (**2013**). "Toward a time domain approach to the linear sampling method," Inverse Problems **29**(9), 095016.
Guzina, B. B., and Madyarov, A. I. (**2007**). "A linear sampling approach to inverse elastic scattering in piecewise-homogeneous domains," Inverse Problems **23**(4), 1467.
Haddar, H., Lechleiter, A., and Marmorat, S. (**2014**). "An improved time domain linear sampling method for Robin and Neumann obstacles," Applicable Anal. **93**(2), 369–390.
Halliday, D., and Curtis, A. (**2008**). "Seismic interferometry, surface waves and source distribution," Geophys. J. Int. **175**(3), 1067–1087.
Larose, E., Margerin, L., Derode, A., van Tiggelen, B., Campillo, M., Shapiro, N., Paul, A., Stehly, L., and Tanter, M. (**2006**). "Correlation of random wavefields: An interdisciplinary review," Geophysics **71**(4), SI11–SI21.
Lobkis, O. I., and Weaver, R. L. (**2001**). "On the emergence of the Green's function in the correlations of a diffuse field," J. Acoust. Soc. Am. **110**(6), 3011–3017.
Lumley, D. E. (**2001**). "Time-lapse seismic reservoir monitoring," Geophysics **66**(1), 50–53.
McMechan, G. A. (**1983**). "Migration by extrapolation of time-dependent boundary values," Geophys. Prospect. **31**(3), 413–420.
Prunty, A. C., and Snieder, R. K. (**2019**). "Theory of the linear sampling method for time-dependent fields," Inverse Problems **35**(5), 055003.
Prunty, A. C., and Snieder, R. K. (**2020**). "An acoustic Lippmann-Schwinger inversion method: Applications and comparison with the linear sampling method," J. Phys. Commun. **4**(1), 015007.
Rajan, S. D., and Frisk, G. V. (**2020**). "Estimation of three-dimensional water column sound speed profiles and sediment compressional wave speed and density profiles using a distributed network of buoys," J. Acoust. Soc. Am. **147**(3), 1392–1403.
Roux, P., Kuperman, W., and the NPAL Group. (**2004**). "Extracting coherent wave fronts from acoustic ambient noise in the ocean," J. Acoust. Soc. Am. **116**(4), 1995–2003.
Sabra, K., Gerstoft, P., Roux, P., Kuperman, W., and Fehler, M. (**2005**). "Surface wave tomography from microseisms in Southern California," Geophys. Res. Lett. **32**, L14311, https://doi.org/10.1029/2005GL023155.
Sabra, K. G., Srivastava, A., Lanza di Scalea, F., Bartoli, I., Rizzo, P., and Conti, S. (**2008**). "Structural health monitoring by extraction of coherent guided waves from diffuse fields," J. Acoust. Soc. Am. **123**(1), EL8–EL13.
Schneider, W. A. (**1978**). "Integral formulation for migration in two and three dimensions," Geophysics **43**(1), 49–76.
Sens-Schönfelder, C., and Wegler, U. (**2006**). "Passive image interferometry and seasonal variations of seismic velocities at Merapi Volcano, Indonesia," Geophys. Res. Lett. **33**(21), L21302, https://doi.org/10.1029/2006GL027797.
Shapiro, N. M., and Campillo, M. (**2004**). "Emergence of broadband Rayleigh waves from correlations of the ambient seismic noise," Geophys. Res. Lett. **31**(7), L07614, https://doi.org/10.1029/2004GL019491.
Shapiro, N. M., Campillo, M., Stehly, L., and Ritzwoller, M. H. (**2005**). "High-resolution surface-wave tomography from ambient seismic noise," Science **307**(5715), 1615–1618.
Snieder, R. (**2006**). "Retrieving the Green's function of the diffusion equation from the response to a random forcing," Phys. Rev. E **74**(4), 046620.
Snieder, R. (**2007**). "Extracting the Green's function of attenuating heterogeneous acoustic media from uncorrelated waves," J. Acoust. Soc. Am. **121**(5), 2637–2643.
Snieder, R., and Larose, E. (**2013**). "Extracting Earth's elastic wave response from noise measurements," Annu. Rev. Earth Planet. Sci. **41**(1), 183–206.
Snieder, R., Wapenaar, K., and Wegler, U. (**2007**). "Unified Green's function retrieval by cross-correlation: Connection with energy principles," Phys. Rev. E **75**(3), 036103.
Tacchino, A., Coyle, J., and Piana, M. (**2002**). "Numerical validation of the linear sampling method," Inverse Problems **18**(3), 511–527.
Tarantola, A. (**1984**). "Inversion of seismic reflection data in the acoustic approximation," Geophysics **49**(8), 1259–1266.
Vasco, D. W. (**2004**). "Seismic imaging of reservoir flow properties: Time-lapse pressure changes," Geophysics **69**(2), 511–521.
Vasco, D. W., Datta-Gupta, A., Behrens, R., Condon, P., and Rickett, J. (**2004**). "Seismic imaging of reservoir flow properties: Time-lapse amplitude changes," Geophysics **69**(6), 1425–1442.
Virieux, J., and Operto, S. (**2009**). "An overview of full-waveform inversion in exploration geophysics," Geophysics **74**(6), WCC1–WCC26.
Wapenaar, K., Fokkema, J., and Snieder, R. (**2005**). "Retrieving the Green's function in an open system by cross correlation: A comparison of approaches (L)," J. Acoust. Soc. Am. **118**(5), 2783–2786.